Additive Manufacturing 23 (2018) 294–302

Contents lists available at ScienceDirect

Additive Manufacturing

journal homepage: www.elsevier.com/locate/addma

Embedded electrical tracks in 3D printed objects by fused filament fabrication of highly conductive composites

J.C. Tan, H.Y. Low*

Engineering Product Development Pillar, Digital Manufacturing and Design Centre (DManD), Singapore University of Technology and Design, 8 Somapah Road, 487372, Singapore

ARTICLE INFO

Keywords:
Additive manufacturing
Fused filament fabrication
3D printing
Electronics
Conductive filament

ABSTRACT

The incorporation of electrical components into 3D printed products such as sensors or printing of circuits requires the use of 3D printable conductive materials. However, most conductive materials available for fused filament fabrication (FFF) have conductivities of less than 1000 S/m. Here, we describe the study of conductive thermoplastic composites comprising either nylon – 6 or polyethylene (PE) matrix. The fillers used were nickel and Sn95Ag4Cu1, a low melting point metal alloy. The combination of nickel metal particles and tin alloy allows for higher metal loading at lower melt viscosity, compared to composites of nickel metal particles alone. Conductivities of 31,000 S/m were achieved, and 30 vol. % metal loading was processable by a single screw extruder. Embedded conductive tracks of various geometries were easily printed via FFF. Electrical conductivity of embedded conductive track has been investigated as a function of geometrical variation, where conductive tracks printed along a horizontal axis show resistance of ≤ 1 Ω. Porosity of the printed track is shown to increase with prints along the vertical axis, leading to a reduction in electrical conductivity of more than two orders of magnitude.

1. Introduction

3-D printing is a unique additive process because a high degree of design customization can be achieved in relatively short turnaround time. A promising application of 3-D printing is in personalized wearable devices, in which a product can be designed according to the user's body features and comfort. Known functional 3D printing materials include; shape-memory [1,2], magnetic [3,4], thermally [5,6] and electrically [7,8] conductive, flexible, biocompatibility [9,10]. Current research has utilized various additive manufacturing techniques and novel materials for prototyping novel wearable technologies for applications such as sensors [7,8], conformal circuits [11–13] and printable antennas [14,15]. In a number of these works, the electrically conductive materials used with 3D printing were extrusion of solvent-based conductive inks, or fused filament fabrication (FFF) printing of polymer composites filled with conductive materials.

Conductive inks have three main components: Micro / nano sized conductive particles; the liquid phase (aqueous or organic); and additives which serve to modify various characteristics such as rheology, surface tension, ink stability and substrate adhesion of the ink for printing. Inks based on noble metals such as silver and gold are typically used due to good electrical conductive properties and chemical inertness in ambient conditions. Recently, there has been increased interest in the use of carbon nanotubes [16,17] and graphene [18,19] as conductive components in ink. Table 1 summarizes a list of recently published work for conductive inks and composites. Although capable of significantly higher electrical conductivity compared to conductive composites, conductive inks have a stricter set of physical requirements when using them for

3D printing processes. One such important requirement in conductive ink 3D printing is the higher viscosity of the ink. In most applications, conductive inks are formulated to contain filler material from 20 to 80 wt. % [26], but 3D printing applications necessitates the usage of conductive inks close to the maximum loading to ensure shape retention of the printed ink, as well as avoid drying-induced shrinkage and cracking due to the evaporation of solvent [27–29]. Another important processing criterion is a fast solvent drying rate. For successful layer by layer 3D printing, the previously deposited layer is required to retain its shape and must be able to support additional layers deposited thereafter. Hence, sufficient solvent must be evaporated such that the bottom layer has sufficient yield strength before printing of the subsequent layer can continue [27]. A long drying time in between the deposition of each layer would cause the entire print duration to increase significantly. After the object has been printed, contact between

* Corresponding author.
E-mail address: hongyee_low@sutd.edu.sg (H.Y. Low).

https://doi.org/10.1016/j.addma.2018.06.009
Received 23 April 2018; Received in revised form 11 June 2018; Accepted 12 June 2018
Available online 14 June 2018

Table 1
3D Printable Conductive Inks and Composites.

Material	Conductivity (S/m)	Resistivity (Ω.m)	Loading	Process	References
Copper, steel (20 μm) powder, PLA, DCM	1.4×10^{6} [a]	7.0×10^{-7}	98 wt. %	Ink extrusion, furnace sintered with copper infiltration at 1120 °C	[20]
Ag nanoparticles, aqueous organic mixture	5.1×10^{4}	2.0×10^{-5} [a]	30 wt. %	Ink extrusion on cotton, sintering at 60 °C	[21]
Gold hexanethiol-encapsulated nanoparticles (1.5 nm), toluene	2.9×10^{7} [b]	3.5×10^{-8}	50 wt. %	Inkjet printing on PET, sintering at 150 °C	[11]
CNT/PLA, DCM	2.3×10^{3} [a]	4.3×10^{-4}	30 wt. %	Ink extrusion	[22,23]
Graphene ABS	1.1×10^{-3} [a]	9.5×10^{2}	5.6 wt. %	FFF extrusion	[24]
Graphene PLA (Commercial product)	166.7	6.0×10^{-3} [a]	Undisclosed	FFF extrusion	[25]
Carbon black PCL	10	0.1 [a]	15 wt. %	FFF extrusion	[7]
Carbon black PP	200	5.0×10^{-3} [a]	40 wt. %	FFF extrusion	[8]

[a] denotes electrical values reported directly from listed references.
[b] reported as 70% conductivity of bulk gold.

the conductive particles usually remains poor due to residual organic stabilizing agents and other added components, which results in high contact resistance between particles. In such cases of high resistance, application of a large current ($> 1.56\ mA/\mu m^2$) results in failure of the ink printed conductive track due to excessive thermal energy [30]. An additional sintering process is performed to weld the metal particles together, which leads to increased electrical conductivity of the printed product [26,31,32]. Compared to bulk metal, metal nanoparticle sintering occurs at much lower temperatures (Table 1), due to the high surface to volume ratio of the particles, which allows for surface diffusion to readily occur between particles [33]. Although sintering temperatures of less than 100 °C have been achieved, it remains a necessary post-processing step for the production of high conductivity structures after ink printing [21,34].

On the other hand, conductive FFF printable materials typically consist of thermoplastic polymer mixed with conductive filler at sufficiently high loading to form a conductive percolated network. In FFF printing, the materials are deposited in a molten state by being extruded through a movable heated nozzle in a specific layout to form a layer, with subsequent layers deposited on top to form a 3D object. As no solvents are used in the FFF material, prints do not experience long drying times and significant volume changes due to solvent evaporation. Although a number of research groups have used various forms of carbon as filler materials for 3D printing filament such as nanotubes [35,36], graphene sheets [24,25], carbon black nanoparticles [7,8], the volume conductivities are lower than ~ 200 S/m, due primarily to carbon's relatively low intrinsic conductivity. Metals, which have much higher conductivity than carbon, are an alternative filler to improve the conductivity of composites. However, current 3D printable metal composites are limited to low filler loadings due to processing difficulties, and are typically for used for aesthetic purposes (colour, texture) as they are non-conductive. Additionally, FFF printing of conductive thermoplastic composites can be difficult due to a variety of reasons. Some of these include; increased viscosity due to high filler loading, high tendency for nozzle clogging, increased warping of the print object while printing, detachment of object from print bed, and decreased quality of print due to nozzle fouling, among others [7,8,24,25,35,36]. Furthermore, ink-based printing processes are not easily adaptable for embedded architecture, in other words, the printing of ink-based conductive track is mostly limited to the surface a printed object.

In this paper, the preparation and characterization of metal - filled polymer composite filaments based on high density polyethylene (HDPE) and nylon - 6 is described. The metal filler consists of two metals: 1) Micron-sized nickel powder. 2) Sn95Ag4Cu1 low melting point metal (LMPM) alloy. By replacing a portion of the metal filler with LMPM, the viscosity of the polymer composite melt would be lowered when processed above the melting point of the LMPM. Additionally, the solid Ni particles aid in preventing complete coalescence of the liquid metal to result in a dispersed mixture of LMPM and nickel particulates in a polymer matrix.

2. Materials and methods

2.1. Preparation of conductive polymer composites

Pellets of polycaprolactam – 6 (Scientific Polymers) or high density polyethylene (Sigma Aldrich) was dried in an oven at 60 °C for 48 h prior to use. Nylon-6 metal-filled composites of 5–35 vol. % metal loading were prepared by melt mixing polycaprolactam – 6, nickel powder (-300 mesh, Strem) and LMPM alloy Sn95Ag4Cu1 (Stannol) in a single screw extruder (Laboratory Mixing Extruder, Dynisco). HDPE metal-filled composites of 5–35 vol. % metal loading were prepared by melt mixing polyethylene (High density, melt index 12 g/10 min (190 °C/2.16 kg), Sigma Aldrich), nickel powder (3–7 μm, Strem) and LMPM alloy Sn95Ag4Cu1 in a single screw extruder. For both nylon-6 and HDPE composites, the volume proportion of nickel particles to tin alloy was 2:3.The rotor temperature for nylon and PE mixing was set to 240 °C and 220 °C respectively, and the header was set to 220 °C. The extruder rotor was spun at 50 RPM. A header die size of 1.75 mm in diameter was used to extrude filaments, and they were collected on a customized conveyor belt system moving at the rate of 0.5 mm/second. A 12 V electric fan of size 12 cm × 12 cm was used to cool the filament while being pulled by the conveyor belt. Due to the low mixing volume in the extruder, the ingredients were added in small volumes (approximately 1 ml), but in proportion with matrix and filler. No premixing was performed. In each batch, filaments were collected and repelletized before undergoing another process of melt extrusion. Extrusion was performed three times to ensure homogeneous mixing of composites. Diameters of the conductive filaments extruded were measured to be1.75 ± 0.08 mm using a digital vernier calliper and was directly used for 3D printing (Fig. 1).

2.2. 3D printing

3D printing was performed on a Flashforge Creator Pro with a Mk10 0.4 mm nickel alloy coated nozzle (Micro Swiss). A heated print bed (70 °C) covered with Polycarbonate Board (Flashforge) served as the base for all 3D prints. Conductive composites of HDPE filaments were used in a dual-material FFF printer, and printed in conjunction with non-conductive polylactic acid (PLA) filaments to produce embedded conductive tracks within a 3D object. Conductive HDPE and conductive nylon - 6 composites were printed at a nozzle temperature of 230 °C and 265 °C respectively, while PLA was printed at 190 °C. Other printing parameters such as extrusion ratio, printing speed, infill percentage and layer thickness are 105%, 20 mm/s, 100% and 0.2 mm respectively. Line pattern was used for infill volume printing. All 3D models were drawn and aligned with Solidworks and exported as 3D manufacturing

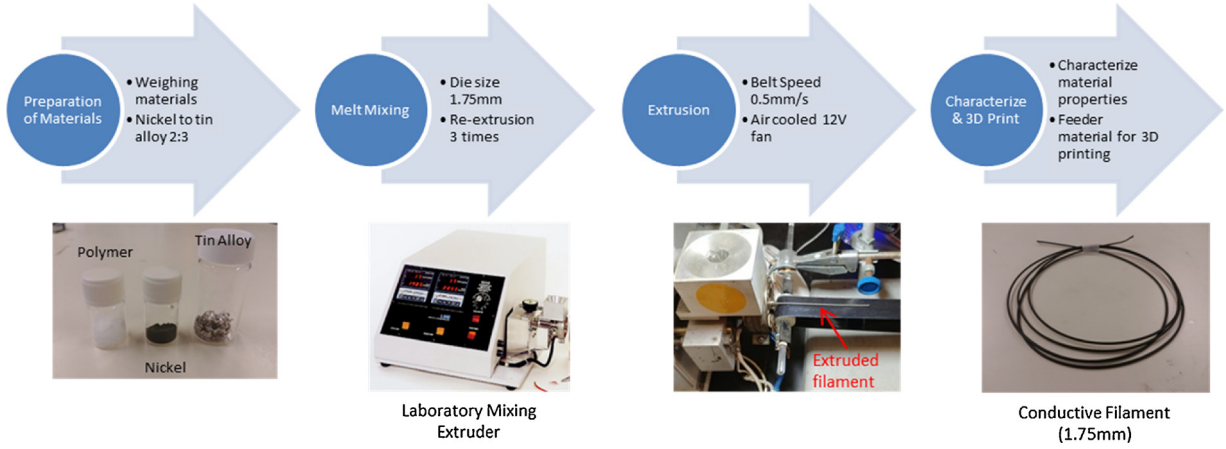

Fig. 1. Melt mixing of polymer (HDPE / Nylon – 6) with nickel powder and tin alloy in an extruder to make an electrically conductive composite. Nickel powder to tin alloy ratio was kept at 2:3. The melt - mixed material was extruded through a 1.75 mm diameter die into filaments. Extruded filaments were re-pelletized and extruded three times to ensure homogeneous mixing. Filaments were then characterised or directly used for as feeder material for FFF printing.

format (.3mf) files. Flashprint (Flashforge) software was then used to slice the. 3mf files into printable format by the FFF printer.

2.3. Measurement of electrical resistivity

A Keithley 6430 source-measurement unit was used to collect electrical resistance data from the conductive filaments and printed products. Electrical measurements were performed using two-point method.

2.4. Measurement of composite melt viscosity

Viscosity of the nylon and HDPE conductive composites were recorded using a Discovery HR-2 (TA Instruments). Samples were loaded between smooth aluminium 25 mm parallel plates, in constant rotational, stress controlled mode. For HDPE composites, samples were heated up to 150 °C and held at that temperature for 30 s before commencement of viscosity readings. Viscosity measurements were performed from 150 °C to 240 °C at a shear rate of 1 1/s. For nylon – 6 composites, samples were heated up to 220 °C and held at that temperature for 30 s before commencement of viscosity readings. Viscosity measurements were performed from 220 °C to 265 °C at a shear rate of 1 1/s. Temperature ramp rate was 5 °C/min.

2.5. Measurement of composite mechanical strength

Tensile properties of the filaments were measured by a tensile strength tester (Micro Tester 5947, Instron). The specimens were designed according to ASTM D882 suitable for thin films, and the speed of testing was set to 3 mm/min. To fabricate specimens for tensile testing, filaments of conductive composites were hot pressed at 220 °C into films with thickness of 0.5 mm. They were then cut into rectangular pieces measuring 2 cm x 5 cm. For each filler composition, three samples were tested. To load onto the strength tester, specimens were held by pneumatic vice grips with rubber coated inserts, which prevents the film from prematurely breaking at the grip edge and also keeps it from slipping.

2.6. Morphology analysis of filler by scanning electron microscopy (SEM)

To visualize the dispersion of metal fillers in the conductive composites, scanning electron microscopy (JEOL JSM-7600 F) was used. Nylon composite (25 vol. %) and HDPE composite (25 vol. %) filament samples were used for SEM characterization. Specimens were fractured after being cooled in liquid nitrogen to obtain cross sections and were coated with gold/palladium alloy (20 mA, 20 s) and mounted onto a specimen holder with adhesive carbon tape. Imaging was performed with 15 kV accelerating voltage in high vacuum mode. Percentage porosity was obtained using SEM images of the cross-sectioned 3D printed samples and quantification with ImageJ. Quantification was performed by using ImageJ's colour balance threshold. For each respective orientation, three samples were printed with newly compounded 6000 S/m PE composite filament. Each sample was sectioned at three different locations of the sample. For each sectioned location, both sides of the exposed surface were analysed under SEM to ensure that the areas of porosity are not negatives of the opposite surface.

3. Results and discussion

3.1. Material formulation for conductive composites

The conductive fillers consist of nickel particles dispersed in a low melting point metal alloy, Sn95Ag4Cu1. Nickel was chosen due to its high electrical conductivity and resistance to corrosion at room temperature. The tin alloy has a melting temperature of 217 °C, which is within the processing temperatures of the polymers selected in this study. Alloys of Sn have been used as soldering metals in the joining of electric contacts [37]. Sn95Ag4Cu1 shows good wetting characteristics to Ni when molten, which upon solidification, forms a good metal contact with the Ni particles [42,43]. HDPE matrix was selected because it has a melting temperature between 120 °C–140 °C, well within the range of temperatures that can be reached by common FFF 3D printers. Additionally, PE is non-hygroscopic and resistant to chemical attack, and is thermally stable up to 350 °C. Compared to PE, Nylon-6 possesses higher mechanical toughness and is commercially used as a textile material. Additionally, the presence of electronegative groups such as carbonyl groups on nylon-6 has been reported to increase interactions of the polymer with metal surfaces [38–40], which improves the dispersion of metal particles within the nylon matrix during melt mixing. However, a higher melting temperature of 225 °C necessitates a printer hot-end capable of reaching temperatures in excess of 260 °C for FFF printing.

3.1.1. Electrical conductivity of conductive composite

To achieve high conductivity in conductive polymer composites, the volume fraction of conducting material must be sufficiently high to achieve a percolating network throughout the entire volume of the composite, allowing electrons to either tunnel or percolate through the conductive network. This volume fraction, which is known as the percolation threshold, is characterized by a large increase in electrical

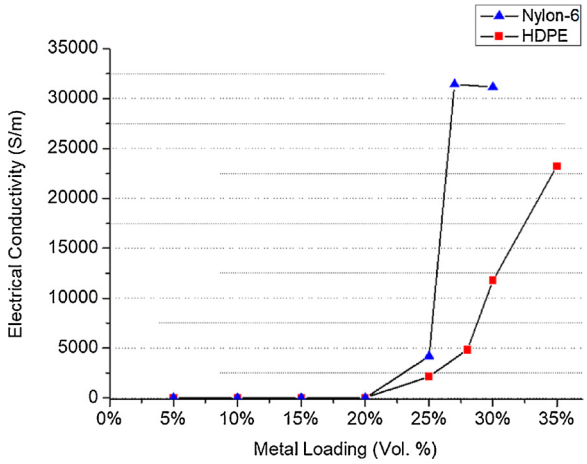

Fig. 2. Relationship between metal loading and electrical conductivity of nylon - 6 metal composites (Blue) and HDPE metal composite filaments (Red). (For interpretation of the references to colour in this figure legend, the reader is referred to the web version of this article.)

conductivity, typically by several orders of magnitude. In this study, electrical resistance of samples were measured using two-point method. Performing resistance readings on embedded conductive tracks using the four-point method proved to be technically challenging. Hence, to maintain consistency between measurements of electrical resistance of filaments and embedded conductive tracks, all electrical measurements adopted the two point method. Samples with metal loadings of 25 vol. % and above were found to be percolated, at which point conductivity increased exponentially from an initially undetectable level to ~4200 S/m (Fig. 2). Upon further addition of metals, electrical conductivity increases to > 31,000 S/m at filler loading of 30 vol. %. As a comparison, the electrical conductivity of bulk copper is 6.0×10^7 S/m, and is a common choice of material in electronics [52]. Nylon - 6 is known to absorb water, leading to changes in dimension and mechanical properties [41]. Water molecules produce polar bonds with the amide groups in the nylon molecules, which results in the nylon matrix swelling. The hygroscopic effect of nylon compromises the electrical conductivity of nylon composites. After extrusion and cooled to room temperature, test filaments (30 vol. %) were left to equilibrate in a 60% R.H. environment at 25 °C for 168 h. At the start of humidity equilibration, the samples were measured to have an average electrical conductivity of 29,000 S/m. After 168 h, conductivity was 21,000 S/m, showing a drop of 25%. The sample filaments were subsequently dried in a 60 °C oven for 48 h, which led to a recovery in conductivity to 28,000 S/m.

Percolation of the HDPE conductive composite was found to be similar to the Nylon conductive composite, i.e. at metal loading of 25 vol. %, electrical conductivity increases exponentially to 23,000 S/m at filler loading of 35 vol. % (Fig. 2). As HDPE is non-hygroscopic, environmental humidity does not affect the electrical conductivity of the composite after melt extrusion. Sample filaments of 30 vol. % exposed to 60% R.H. at 25 °C for 168 h showed no decrease in conductivity.

3.1.2. Effect of LMPM on viscosity

Melt viscosity of the conductive composites is an important parameter for successful FFF printing. Melt extrusion of two-component composite consisting of Ni particles and Nylon - 6 were found to be unsuccessful in achieving percolation, due to difficulties associated with mixing solid Ni particles into molten nylon. Nylon – 6 composites at 15 vol. % were unable to achieve electrical percolation. Additionally, above 15 vol. % loading of Ni, the high loading of solid particulates led to seizing of the extruder, resulting in a non-homogeneously mixed composite sample. The addition of low melting point metals allows for the melt mixing of composites above 15 vol. % metal loading, but at a

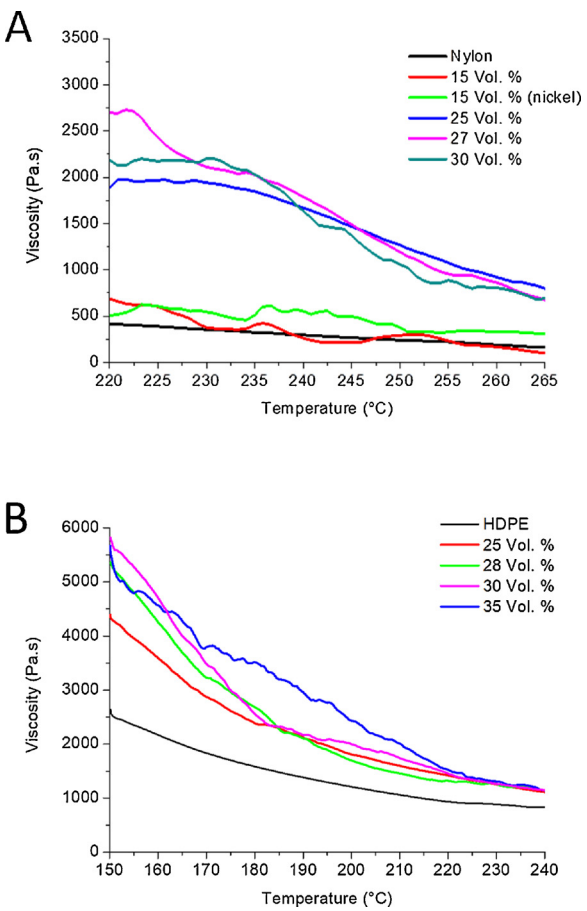

Fig. 3. Viscosity of nylon composites (Top) and PE composites (Bottom) with metal loading of Ni particles and LMPM.

viscosity processable by the single screw extruder [42]. Fig. 3A compares the viscosities of nylon composites of increasing Ni-Sn95Ag4Cu1 loading from temperature of 220 °C to 265 °C at a shear rate of 1 1/s. As shown in Fig. 3A, Nylon-6 composites at metal loadings from 25 to 30 vol. % show a 4–5 fold increase in viscosity compared to the neat Nylon-6 and the 15% vol. filled composite. At higher metal loading, the temperature dependence of the viscosity is non-linear; above 30% vol. of metal loading, melt-extrusion was unsuccessful even at 260 °C.

HDPE has a lower processing temperature than Nylon. Fig. 3B shows the melt viscosity of HDPE composites over a lower temperature range compared to Nylon – 6 composites. Below 210 °C, the Sn alloy exists as solid particles, which explains the relatively high viscosity as shown in Fig. 3B. Above 220 °C, a discernible deflection is seen in viscosity of the PE composite, attributed to the melting of Sn alloy. As such, it was possible to extrude PE conductive composites at 40 vol. % and above. However, the filaments containing above 40 vol. % were highly brittle [46]. This led to excessive breakage of filaments during handling and feeding into the FFF printer.

3.1.3. Morphological analysis of metal filler

SEM images of fractured surfaces from hot pressed composite samples were obtained for analysis of the composite morphologies while elemental map via EDX (Energy-dispersive X-ray spectroscopy) provide chemical distribution in the fractured surfaces. Cross sections SEM image the Nylon-Ni-Sn alloy composite (Fig.4A) shows a rough fractured surface that comprises of metallic particles moderately distributed in the matrix. The EDX maps of Ni and Sn show that the Ni particles (average size 25 μm) are distributed uniformly throughout the matrix. It is also evidenced from Fig. 4C that the Sn cluster overlaps with Ni. An earlier work has reported that during melt extrusion, the

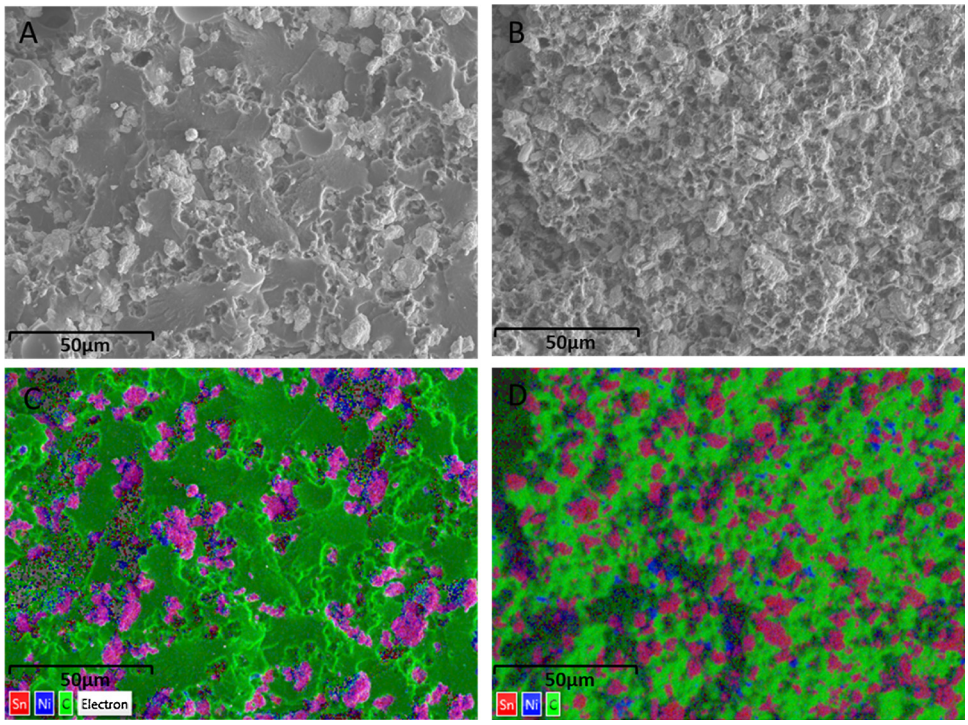

Fig. 4. SEM images of fractured surfaces: A) 25 vol. % nylon composite. B) 25 vol. % PE composite. C EDX map of Ni, Sn and C overlaid onto SEM images in (A), blue, red and green are Ni, Sn and carbon signals respectively. D) EDX map of Sn, Ni and C overlaid onto SEM image in (B), red clusters are Sn, blue clusters are Ni and green background are carbon signals. The appearance of purple in the image is due to the co-localization of red and blue signals, indicating the interaction between Ni and Sn. (For interpretation of the references to colour in this figure legend, the reader is referred to the web version of this article.)

liquid Sn alloy preferentially wets the surface of the nickel particles [43], a critical factor for reducing coalescence of liquid Sn particles. While the Sn particles are in a molten state, intermetallic bonds are formed between Ni and Sn, and upon cooling, the liquid Sn alloy solidifies around the nickel particles, creating a well-bonded interface [43,44]. Also apparent in the SEM-EDX image is the presence of dispersed Ni particles between the clusters of metal particles, which forms the percolated network structure.

The PE composite samples loaded with 28 vol. % metals show similar morphology as the Nylon composite. Fig. 4B shows the metallic particles are distributed throughout the exposed surface and the metal cluster sizes range from 5 to 20 µm. Fig. 4D shows an SEM image of the same filament fragment, along with elemental maps obtained from EDX for Ni (blue) and Sn (red). Similar to nylon composites, the EDX image indicates that the Ni and Sn particles are co-localized, attributed to the encapsulation of Ni by Sn. The similarities in the morphology and distribution of the metal fillers in Nylon and PE matrix, as shown by the EDX - SEM images, corroborate with the conductivity measurement, in which both composites are found to percolate at the metal loading of about 25%.

3.1.4. Mechanical properties of conductive composite

Materials used for wearable electronics are required to possess strength and flexibility. However, it has been reported that mechanical properties of 3-D printed parts often suffers a degraded mechanical strength compared to the pristine materials [46,47]. Here, the tensile strength of our composite materials with different metal loadings was investigated. Fig. 5 shows the stress strain curve of nylon and PE samples with increasing metal loading. For nylon composites, the Young's moduli and ultimate tensile stress (UTS) of metal filled samples were increased as a result of metal loading. Young's moduli of metal loaded samples were at least 300% higher than neat nylon, resulting in a stiffer material. Composites of metal-filled PE experienced 50–110% increase in Young's moduli, while the UTS of percolated PE composite samples was found to be lower than neat PE, and toughness was $< 3\ kJ/m^2$.

PE composites of 40 vol. % and above were found to be highly brittle and fragile, with frequent breakage occurring during handling and 3D printing. Due to the highly fragile nature, samples were found to break upon loading onto the clamps of the tensile strength tester, and were unable to be successfully tested for tensile strength. Although the measured Young's moduli, UTS and toughness do not increase linearly with increasing metal loadings, the general trend in the increase in Young's moduli, UTS and the decrease in toughness values are in general agreement with common observations of metal particles filled polymer composites. Composites with metal loadings below the percolation threshold exhibit the highest UTS among the samples tested. A similar trend is seen in the material toughness of composites, where samples with filler loading above the percolation threshold suffer a decrease in total toughness [48,49]. The mechanical properties of conductive composites play a significant role in the successful application of such materials in wearable technology. For the motivation of the current work, nylon composite with 30 vol. % is optimal in its electrical conductivity; the higher UTS than neat nylon is also a desirable property, however, the increase in stiffness and the compromised toughness are not desirable for wearable devices. PE composite of 35 vol. % exhibited good electrical conductivity, with suitable viscosity for FDM printing, although the low toughness contributes to fragility of the material.

3.2. FFF printing of conductive composite

The ability of printing embedded conductive tracks within a structure or device provides several benefits such as reducing the total number of individual components required, and protection of the electrical circuit from mechanical damage. Preliminary printing trials were performed to understand aspects of printing conductive HDPE such as print bed adherence, layer to layer adherence, warping of part, nozzle fouling/clogging. For this study, orientation of the print direction was investigated with respect to the printed conductivity, while keeping printing conditions constant. A dual material FFF printer was used to print simple geometric shapes with an embedded conductive track. Conductive HDPE composite was printed together with non – conductive matrix, PLA. Fig. 6 shows the CAD models of cuboidal structures containing the internal track. Anisotropic effects of printing direction on electrical conductivity were compared against conductive

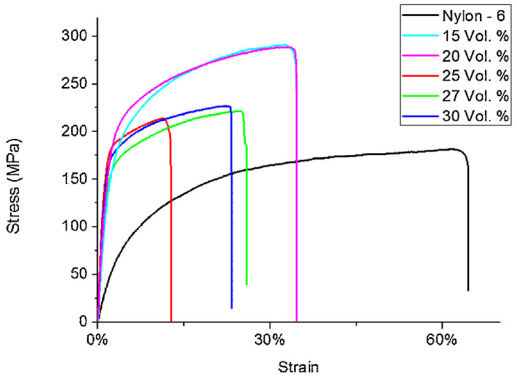

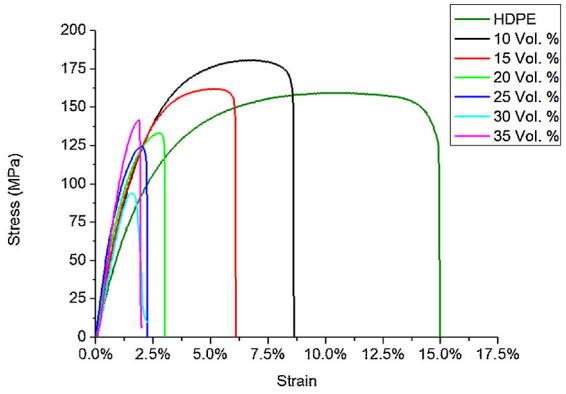

Nylon – 6 Composite Metal Loading	Young's Modulus (GPa)	Ultimate Stress (MPa)	Toughness (kJ/m^2)
0%	2.4	180	97.0
15%	7.8	290	85.8
20%	9.1	280	86.2
25%	12.0	210	24.0
27%	8.1	220	50.1
30%	10.4	220	46.9

HDPE Composite Metal Loading	Young's Modulus (GPa)	Ultimate Stress (MPa)	Toughness (kJ/m^2)
0%	5.1	159	20.1
10%	7.6	180	12.5
15%	7.9	162	7.7
20%	8.5	133	2.8
25%	9.7	124	1.9
30%	7.8	94	1.2
35%	12.3	141	1.7

Fig. 5. Stress strain curve of PE (Top left) and nylon (Top right) metal composites, with tables summarizing (Bottom) Young's modulus, ultimate tensile stress and toughness of metal composites from the respective stress strain curves.

tracks printed from HDPE filaments of various conductivities. The designs were printed with the longest side along either of the horizontal (X/Y) axes, vertical (Z) axis, or across all three axes (XYZ). Fig. 6 also lists the conductivity values of filaments, embedded conductive tracks, and the percentage retention of electrical conductivity from filament to print. The conductivities of embedded conductive tracks in dual material composition decreased from 1 to 2 orders of magnitude compared to the extruded, pre-printing filament. However, the drop in electrical conductivity is lowest in conductive tracks printed with the highest conductive filaments along the horizontal axis (11.6% retention of conductivity). The retention in electrical conductivity increases as a more conductive filament was used (Fig. 6). As the phenomena of conduction in composites requires close proximity between the conducting metal particles, the retention of conductivity after printing is similarly dictated by the surface contact of metal particles between the stacked layers. Filaments of higher conductivity contain higher number of metal particles which when printed, increases the probability of metal particle contact between the stacked layers.

When the conductive tracks were printed in the X/Y axis, nozzle extrusion proceeds without interruption during printing of a layer, conductive tracks along the X/Y axis will also consist of a continuous structure, which results in conductance along the layer. On the other hand, conductive tracks proceeding along the Z axis requires deposition of material in a layer-by-layer step, and conductivity retention is dependent on contact/interfacial adhesion between layers of deposited material. The FFF printing process is known to introduce voids and air gaps into objects printed with up to 8% porosity, even when printing fully filled objects [50]. With conventional printing materials such as acrylonitrile butadiene styrene (ABS) and PLA, porosity of the printed object is judiciously tailored to suit the mechanical properties required by the printed object, and to minimize wastage of printing material. However, in the printing of conductive materials, porosity affects the electrical conductivity of the printed composite. In previous studies, it was shown that conductive circuits printed using FFF techniques would experience a drop in electrical conductivity of up to two orders of magnitude after printing [24]. As FFF produces 3D objects by depositing thermoplastic material onto a stage in layers, voids inevitability exist within the printed model, and adjacent fibres may not be completely fused, leading to a reduction in volume conductivity.

To investigate the porosity of the printed conductive track with respect to track orientation, cross-sections of conductive tracks were analysed with SEM imaging. Fig. 7 shows the cross-sectional SEM image of printed PLA cuboids (5 mm × 5 mm × 20 mm) embedded with a straight HDPE composite conductive track (3 mm × 3 mm × 20 mm). High magnification image of the horizontal conductive track seen in Fig. 7 show similar morphology and distribution of the metallic filler particles to the HDPE composite filaments in Fig. 4. Voids are clearly discerned from the cross-sectioned image. Using a total of nine different cross-sections obtained from three printed samples, porosity in the horizontally printed conductive HDPE track was measured to be an average of 12% ± 0.4%. The presence of undesired air gaps in the conductive track is a significant detriment to the electrical properties of the printed object. Non-uniform porosity within the printed conductive structure creates voids in the percolation network, leading to a drop in electrical conductivity. Print orientation of the conductive track has a marked effect on the porosity of the structure. Objects that were printed along the vertical and diagonal axes showed increasing porosity of 25% and 32% respectively (Fig. 7), which corresponds with the decreasing conductivity of tracks printed along those respective orientations as shown in Fig. 6. The porosity introduced during the printing process is the result of insufficient deposition of extruded material, of which could be due to a number of reasons such as slow extrusion rate and thermal shrinkage during cooling. Additionally, it was observed that at random intervals during the printing of vertical conductive tracks, extruded conductive material would adhere onto the tip of the printing nozzle to form a viscous non-deposited residue droplet. With subsequent nozzle movements during printing, this residue droplet randomly coalesces with sections of the build piece, removing minute amounts of previously deposited conductive material from the object undergoing printing, resulting in porosity. This suggests that viscosity of the conductive composite melt during the printing process plays a role in the outcome of printing conductive structures. As the majority of wearable articles should conform to the wearer's individualized body shape and motion, materials used in such applications have a strict requirement of being able to undergo bending, twisting and stretching. The Young's modulus of conductive composites, although reaching the higher end of

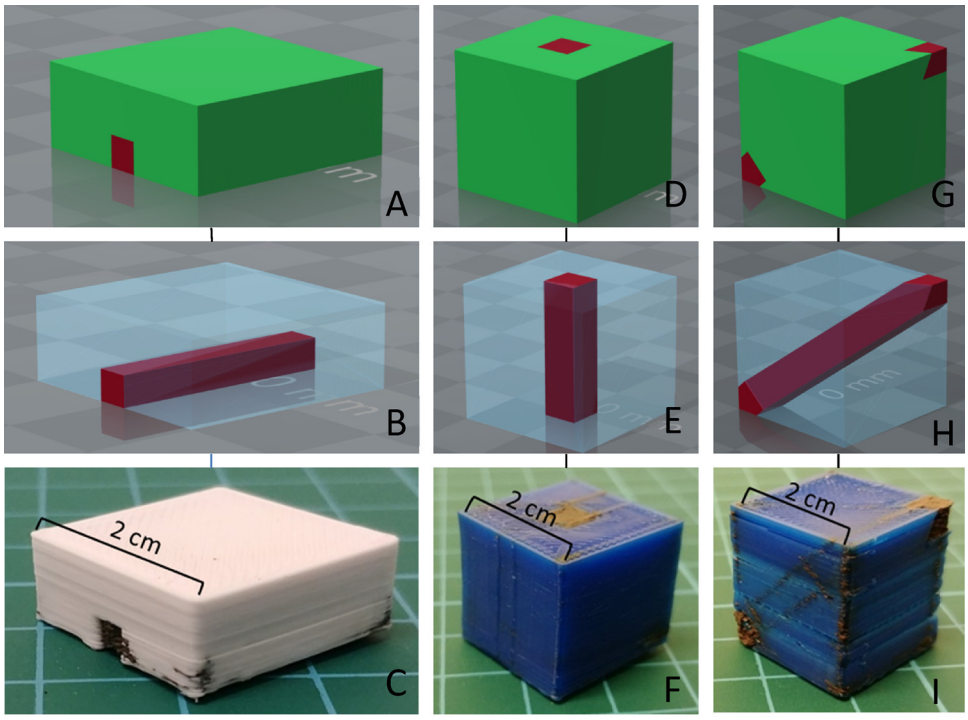

Fig. 6. Computer aided design models for dual material printing of a conductive track (dark red) through a non-conductive print medium (green) in the horizontal axis (X/Y) (A), vertical axis (Z) (D), and across all three axes (XYZ) (G). (B, E, H) Internal view of the print models rendered with non-conductive regions transparent. (C, F, I) Printed copies of the models with conductive tracks along their respective axes. Table shows the measured conductivity of the conductive track, and the filaments used in the printing of each respective track (Bottom). (For interpretation of the references to colour in this figure legend, the reader is referred to the web version of this article.)

Track Axis	Dimensions of Track (mm) L x W x H	Resistance (Ω)	Conductivity (S/m)	Filament Conductivity (S/m)	Filament to Print Conductivity Retention
X/Y	3 x 3 x 20	28	80	2400	3.3%
X/Y	3 x 3 x 20	4	530	10000	5.3%
X/Y	3 x 3 x 20	1	1850	16000	11.6%
X/Y	12 x 0.8 x 20	1	1810	16000	11.3%
Z	5 x 5 x 20	472	2	2400	0.07%
Z	5 x 5 x 20	21	40	10000	0.4%
Z	5 x 5 x 20	2	380	16000	2.4%
X Y Z	5 x 5 x 35	2	820	21000	3.9%

stiffer polymers [51], can be shaped into specific geometries through the use of FFF printing and judicious designs. This enables them to yield to bending, twisting and stretching forces which fabric materials might be subjected to. However, the current work does not investigate how electrical conductivity might change with application of those stresses. For practical reasons, the ability for the composite to retain similar levels of electrical conductivity while being subjected to flexing is crucial for the functionality of wearable devices used in conjunction with conductive composites. Future work will attempt to improve upon the composite electrical conductivity, and investigate how conductivity of the composites will be affected by stresses applied by various forms of flexing.

4. Conclusion

This work describes the formulation and characterization of conductive composites based on matrix materials nylon – 6 and PE, filled with metals Ni and low melting point Sn alloy. For nylon – 6, conductivity of $\sim 3.1 \times 10^4$ S/m was achieved with metal loadings of 30 vol. %. As nylon -6 is hygroscopic, interaction of the composites with a humid environment led to a decrease in electrical conductivity. The decrease in conductivity could be reversed by drying the composite in a 60 °C oven for 48 h. PE composites achieved conductivity of 23,000 S/m at filler loading of 35 vol. %. As polyethylene matrix is non-hygroscopic, environmental humidity does not affect the electrical conductivity of the composite after extrusion. The addition of LMPM allows for a higher metal loading to be achieved (30 vol. %), compared to filling with solid metal fillers (15 vol. %). Dual-material models were successfully printed with non-conductive PLA and conductive PE to create simple objects with 3D conductive tracks. Print direction was found to substantially compromise the conductivity of the composite due to the formation of voids; printing along the X/Y axis allowed for a higher retention of electrical conductivity of the resulting 3D printed conductive track. Research is on-going to increase the retention in the conductivity of FFF printed tracks by reducing the void formation, through reducing the variability of the filament diameter to maintain a steady extrusion rate during printing, and increasing adherence between printed paths and layers by increasing printing temperature or by reducing the rate of cooling.

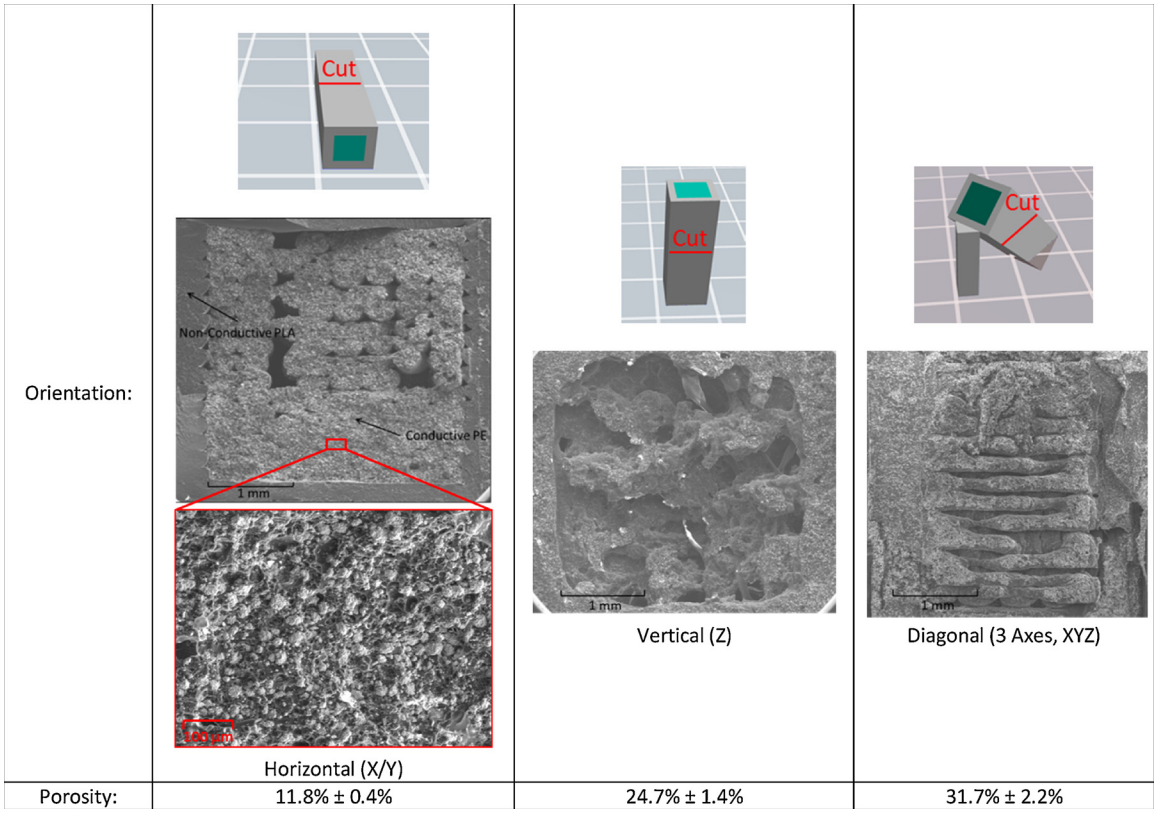

Fig. 7. Cross-section images of printed samples with different print orientations exposed through brittle fracture. (Top) CAD model showing orientation of fracture line. (Bottom) SEM image of the exposed cross-sectional area. Porosity was quantified as the percentage area of voids against the total cross-section area of the conductive tracks (3 mm × 3 mm).

Acknowledgement

This work was supported by the Singapore University of Technology and Design (SUTD), and funded in part by the Digital Manufacturing and Design Centre, SUTD. The authors would also like to acknowledge PhD. student Ong Shike for her contributions and advice to the CAD models used in this work.

References

[1] Y. Yang, Y. Chen, Y. Wei, Y. Li, 3D printing of shape memory polymer for functional part fabrication, Int. J. Adv. Manuf. Technol. 84 (9–12) (2016) 2079–2095.
[2] F.S. Senatov, K.V. Niaza, M.Y. Zadorozhnyy, A.V. Maksimkin, S.D. Kaloshkin, Y.Z. Estrin, Mechanical properties and shape memory effect of 3D-printed PLA-based porous scaffolds, J. Mech. Behav. Biomed. Mater. 57 (2016) 139–148.
[3] S.J. Leigh, C.P. Purssell, D.R. Billson, D.A. Hutchins, Using a magnetite/thermoplastic composite in 3D printing of direct replacements for commercially available flow sensors, Smart Mater. Struct. 23 (9) (2014) 095039.
[4] M.M. Stanton, C. Trichet-Paredes, S. Sanchez, Applications of three-dimensional (3D) printing for microswimmers and bio-hybrid robotics, Lab Chip 15 (7) (2015) 1634–1637.
[5] U. Kalsoom, A. Peristyy, P.N. Nesterenko, B. Paull, A 3D printable diamond polymer composite: a novel material for fabrication of low cost thermally conducting devices, RSC Adv. 6 (44) (2016) 38140–38147.
[6] C. Shemelya, A. De La Rosa, A.R. Torrado, K. Yu, J. Domanowski, P.J. Bonacuse, B. Conner, et al., Anisotropy of thermal conductivity in 3D printed polymer matrix composites for space based cube satellites, Addit. Manuf. 16 (2017) 186–196.
[7] S.J. Leigh, R.J. Bradley, C.P. Purssell, D.R. Billson, D.A. Hutchins, A simple, low-cost conductive composite material for 3D printing of electronic sensors, PloS One 7 (11) (2012) e49365.
[8] S.W. Kwok, K.H.H. Goh, Z.D. Tan, S.T.M. Tan, W.W. Tjiu, J.Y. Soh, K.E.J. Goh, et al., Electrically conductive filament for 3D-printed circuits and sensors, Appl. Mater. Today 9 (2017) 167–175.
[9] E. Sachlos, J.T. Czernuszka, Making tissue engineering scaffolds work. Review: the application of solid freeform fabrication technology to the production of tissue engineering scaffolds, Eur. Cell Mater. 5 (29) (2003) 39–40.
[10] D.W. Hutmacher, T. Schantz, I. Zein, K.W. Ng, S.H. Teoh, K.C. Tan, Mechanical properties and cell cultural response of polycaprolactone scaffolds designed and fabricated via fused deposition modeling, J. Biomed. Mater. Res. A 55 (2) (2001) 203–216.
[11] D. Huang, F. Liao, S. Molesa, D. Redinger, V. Subramanian, Plastic-compatible low resistance printable gold nanoparticle conductors for flexible electronics, J. Electrochem. Soc. 150 (7) (2003) G412–G417.
[12] L. Hu, M. Pasta, F. La Mantia, L. Cui, S. Jeong, H.D. Deshazer, Y. Cui, et al., Stretchable, porous, and conductive energy textiles, Nano Lett. 10 (2) (2010) 708–714.
[13] T.H. Van Osch, J. Perelaer, A.W. de Laat, U.S. Schubert, Inkjet printing of narrow conductive tracks on untreated polymeric substrates, Adv. Mater. 20 (2) (2008) 343–345.
[14] M. Liang, C. Shemelya, E. MacDonald, R. Wicker, H. Xin, 3-D printed microwave patch antenna via fused deposition method and ultrasonic wire mesh embedding technique, IEEE Antennas Wirel. Propag. Lett. 14 (2015) 1346–1349.
[15] P. Deffenbaugh, K. Church, J. Goldfarb, X. Chen, Fully 3D printed 2.4 GHz bluetooth/wi-Fi antenna, January, No. 1, International Symposium on Microelectronics vol. 2013, International Microelectronics Assembly and Packaging Society, 2013, pp. 000914–000920.
[16] J.W. Song, Y.S. Kim, Y.H. Yoon, E.S. Lee, C.S. Han, Y. Cho, H.T. Jung, et al., The production of transparent carbon nanotube field emitters using inkjet printing, Phys. E: Low-Dimen. Systems Nanostruct. 41 (8) (2009) 1513–1516.
[17] S. Azoubel, S. Shemesh, S. Magdassi, Flexible electroluminescent device with inkjet-printed carbon nanotube electrodes, Nanotechnology 23 (34) (2012) 344003.
[18] L. Huang, Y. Huang, J. Liang, X. Wan, Y. Chen, Graphene-based conducting inks for direct inkjet printing of flexible conductive patterns and their applications in electric circuits and chemical sensors, Nano Res. 4 (7) (2011) 675–684.
[19] L.T. Le, M.H. Ervin, H. Qiu, B.E. Fuchs, W.Y. Lee, Graphene supercapacitor electrodes fabricated by inkjet printing and thermal reduction of graphene oxide, Electrochem. Commun. 13 (4) (2011) 355–358.
[20] C. Xu, A. Bouchemit, G. L'Espérance, L.L. Lebel, D. Therriault, Solvent-cast based metal 3D printing and secondary metallic infiltration, J. Mater. Chem. C (2017).
[21] Z. Wang, W. Wang, Z. Jiang, D. Yu, Low temperature sintering nano-silver conductive ink printed on cotton fabric as printed electronics, Prog. Org. Coat. 101 (2016) 604–611.
[22] K. Chizari, M.A. Daoud, A.R. Ravindran, D. Therriault, 3D printing of highly conductive nanocomposites for the functional optimization of liquid sensors, Small 12 (44) (2016) 6076–6082.
[23] K. Chizari, M. Arjmand, Z. Liu, U. Sundararaj, D. Therriault, Three-dimensional printing of highly conductive polymer nanocomposites for EMI shielding applications, Mater. Today Commun. 11 (2017) 112–118.
[24] X. Wei, D. Li, W. Jiang, Z. Gu, X. Wang, Z. Zhang, Z. Sun, 3D printable graphene composite, Sci. Rep. 5 (2015).
[25] B.M. 3D conductive graphene filament [Internet], Black Magic 3D, Calverton,NY.

Available from: http://graphenelab.com/blackmagic3d/Filaments/Conductive Graphene Filament 216x.pdf [accessed 05.07.17].
[26] S. Magdassi (Ed.), The Chemistry of Inkjet Inks, World scientific, Singapore, 2010p. 3.
[27] A. Kamyshny, S. Magdassi, Conductive nanomaterials for printed electronics, Small 10 (17) (2014) 3515–3535.
[28] J.I.I.I. Cesarano, R. Segalman, P. Calvert, Robocasting provides moldless fabrication from slurry deposition, Ceram. Ind. 148 (4) (1998).
[29] J.A. Lewis, J.E. Smay, J. Stuecker, J. Cesarano, Direct ink writing of three-dimensional ceramic structures, J. Am. Ceram. Soc. 89 (12) (2006) 3599–3609.
[30] D.A. Roberson, R.B. Wicker, E. MacDonald, Microstructural characterization of electrically failed conductive traces printed from Ag nanoparticle inks, Mater. Lett. 76 (2012) 51–54.
[31] D.A. Roberson, R.B. Wicker, L.E. Murr, K. Church, E. MacDonald, Microstructural and process characterization of conductive traces printed from Ag particulate inks, Materials 4 (6) (2011) 963–979.
[32] J. Perelaer, B.J. de Gans, U.S. Schubert, Ink-jet printing and microwave sintering of conductive silver tracks, Adv. Mater. 18 (16) (2006) 2101–2104.
[33] S. Iwama, K. Hayakawa, Sintering of ultrafine metal powders. II. Neck growth stage of Au, Ag, Al and Cu, Jpn. J. Appl. Phys. 20 (2) (1981) 335.
[34] D. Huang, F. Liao, S. Molesa, D. Redinger, V. Subramanian, Plastic-compatible low resistance printable gold nanoparticle conductors for flexible electronics, J. Electrochem. Soc. 150 (7) (2003) G412–G417.
[35] M.L. Shofner, F.J. Rodríguez-Macías, R. Vaidyanathan, E.V. Barrera, Single wall nanotube and vapor grown carbon fiber reinforced polymers processed by extrusion freeform fabrication, Compos. Part A: Appl. Sci. Manuf. 34 (12) (2003) 1207–1217.
[36] F. Ning, W. Cong, J. Qiu, J. Wei, S. Wang, Additive manufacturing of carbon fiber reinforced thermoplastic composites using fused deposition modeling, Compos. Part B-Eng. 80 (2015) 369–378.
[37] S. Jin, Developing lead-free solders: a challenge and opportunity, JOM J. Miner., Metals Mater. Soc. 45 (7) (1993) 13.
[38] K.L. Mittal, Polymer Surface Modification: Relevance to Adhesion vol. 5, CRC Press, 2004.
[39] J.M. Burkstrand, Metal-polymer interfaces: adhesion and x-ray photoemission studies, J. Appl. Phys. 52 (7) (1981) 4795–4800.
[40] L. Delle Site, C.F. Abrams, A. Alavi, K. Kremer, Polymers near metal surfaces: selective adsorption and global conformations, Phys. Rev. Lett. 89 (15) (2002) 156103.
[41] J.W. Hearle, W.E. Morton, Physical Properties of Textile Fibres, Elsevier, 2008.
[42] R.A. Mrozek, P.J. Cole, L.A. Mondy, R.R. Rao, L.F. Bieg, J.L. Lenhart, Highly conductive, melt processable polymer composites based on nickel and low melting eutectic metal, Polymer 51 (14) (2010) 2954–2958.
[43] W.H. Tao, C. Chen, C.E. Ho, W.T. Chen, C.R. Kao, Selective interfacial reaction between Ni and eutectic BiSn lead-free solder, Chem. Mater. 13 (3) (2001) 1051–1056.
[44] P. Nash, A. Nash, The Ni− Sn (Nickel-Tin) system, J. Phase Equilib. 6 (4) (1985) 350–359.
[46] A.G. Evans, S. Williams, P.W.R. Beaumont, On the toughness of particulate filled polymers, J. Mater. Sci. 20 (10) (1985) 3668–3674.
[47] S.Y. Fu, X.Q. Feng, B. Lauke, Y.W. Mai, Effects of particle size, particle/matrix interface adhesion and particle loading on mechanical properties of particulate–polymer composites, Compos. Part B-Eng. 39 (6) (2008) 933–961.
[48] I. Durgun, R. Ertan, Experimental investigation of FDM process for improvement of mechanical properties and production cost, Rapid Prototyp. J. 20 (3) (2014) 228–235.
[49] C.J.R. Verbeek, Effect of percolation on the mechanical properties of sand-filled polyethylene composites, J. Thermoplast. Compos. Mater. 20 (2) (2007) 137–149.
[50] J. Zhang, B. Yang, F. Fu, F. You, X. Dong, M. Dai, Resistivity and its anisotropy characterization of 3D-printed acrylonitrile butadiene styrene copolymer (ABS)/Carbon Black (CB) composites, Appl. Sci. 7 (1) (2017) 20.
[51] M.F. Ashby, Y.J.M. Brechet, Designing hybrid materials, Acta Mater. 51 (19) (2003) 5801–5821.
[52] R.A. Matula, Electrical resistivity of copper, gold, palladium, and silver, J. Phys. Chem. Ref. Data 8 (4) (1979) 1147–1298.